

6-1-1994

Spin diffusion in the one-dimensional $s = 1/2$ XXZ model at infinite temperature

Markus Böhm

V. S. Viswanath
University of Rhode Island

Joachim Stolze
University of Rhode Island

Gerhard Müller
University of Rhode Island, gmuller@uri.edu

Follow this and additional works at: https://digitalcommons.uri.edu/phys_facpubs

Citation/Publisher Attribution

Markus Böhm, V.S. Viswanath, Joachim Stolze and Gerhard Müller. *Spin diffusion in the 1D $s=1/2$ XXZ model at infinite temperature*. Phys. Rev. B **49** (1994), 15669-15681.
Available at <http://journals.aps.org/prb/abstract/10.1103/PhysRevB.49.15669>.

This Article is brought to you by the University of Rhode Island. It has been accepted for inclusion in Physics Faculty Publications by an authorized administrator of DigitalCommons@URI. For more information, please contact digitalcommons-group@uri.edu. For permission to reuse copyrighted content, contact the author directly.

Spin diffusion in the one-dimensional $s = 1/2$ XXZ model at infinite temperature

Publisher Statement

Copyright 1994 The American Physical Society.

Terms of Use

All rights reserved under copyright.

Spin diffusion in the one-dimensional $s = \frac{1}{2}$ XXZ model at infinite temperature

Markus Böhm

Institut für Theoretische Physik, Universität Erlangen-Nürnberg, D-91058 Erlangen, Germany

V. S. Viswanath, Joachim Stolze,* and Gerhard Müller

Department of Physics, The University of Rhode Island, Kingston, Rhode Island 02881-0817

(Received 26 April 1993)

Time-dependent spin-autocorrelation functions at $T = \infty$ and (in particular) their spectral densities for the bulk spin and the boundary spin of the semi-infinite spin- $\frac{1}{2}$ XXZ model (with exchange parameters $J_x = J_y \equiv J, J_z$) are investigated on the basis of (i) rigorous bounds in the time domain and (ii) a continued-fraction analysis in the frequency domain. We have found strong numerical evidence for spin diffusion in quantum spin models. For J_z/J increasing from zero, the results of the short-time expansion indicate a change of the bulk-spin xx -autocorrelation function from Gaussian decay to exponential decay. The continued-fraction analysis of the same dynamic quantity signals a change from exponential decay to power-law decay as J_z/J approaches unity and back to a more rapid decay upon further increase of that parameter. By contrast, the change in symmetry at $J_z/J = 1$ has virtually no impact on the bulk-spin zz -autocorrelation function (as expected). Similar contrasting properties are observable in the boundary-spin autocorrelation functions.

I. INTRODUCTION

After more than two decades of theoretical studies devoted to high-temperature dynamics of quantum spin chains, which have produced a number of intriguing exact results, one central question has remained unanswered: Does the phenomenological concept of spin diffusion provide at all an adequate description for the transport of the fluctuations of a conserved magnetization component? While the spin-diffusion phenomenon was frequently invoked for the interpretation of experimental results from inelastic neutron scattering, electron spin resonance and NMR on quasi-one-dimensional (1D) magnetic compounds,^{1,2} its support by microscopic theories or numerical analysis of quantum spin dynamics has remained rather weak and tentative³⁻⁵ or artificially imposed.⁶

Even for *classical* spin chains, whose long-time dynamics is more readily accessible to numerical analysis by means of simulation studies, the answer to that question has proven to involve unanticipated subtleties. The anomalous character of spin diffusion in the classical Heisenberg chain, identified some five years ago,⁷ has remained a matter of controversy ever since as to its correct interpretation.⁸⁻¹³ There is now strong evidence that the diffusivity is singular, giving rise to logarithmic corrections in the long-time tail of the spin-autocorrelation function,¹² but the exact nature of these corrections and their origin have remained obscure.

It is much more challenging to analyze the long-time dynamics of *quantum* spin chains. There are only very few quantum spin models with nontrivial dynamics for which dynamic correlation functions at $T = \infty$ have been determined exactly. Among them are the equivalent-neighbor XXZ model^{14,15} and the 1D $s = \frac{1}{2}$ XY model.¹⁶⁻²³ Spin diffusion has no part in either model for

reasons that are well understood.

For other quantum spin models with nontrivial dynamics, such as the 1D XXZ model, exact information on dynamic correlation functions is limited to a number of frequency moments obtained from $T = \infty$ expectation values of spin products.^{5,24-26} The information contained in these frequency moments can be employed in two different ways to infer characteristic properties of dynamic correlation functions:

(i) We may use the frequency moments as Taylor coefficients in the short-time expansion of a correlation function. For certain situations, the rigorous upper and lower bounds thus determined for that function may yield accurate results over time intervals that are sufficiently long to unlock valuable information on the underlying physical process—information that is otherwise inaccessible.

(ii) For certain other situations, further information on the long-time behavior can be extracted from the frequency moments if they are converted into an equal number of continued-fraction coefficients for the relaxation function (the Laplace transform of the correlation function).

This paper builds principally on the accomplishments of two previous studies of $T = \infty$ quantum spin dynamics^{23,25} with focus on methods (i) and (ii), respectively. Here the analytic and numerical techniques developed in those studies are combined for the specific purpose of elucidating the $T = \infty$ dynamics of the 1D $s = \frac{1}{2}$ XXZ model. The Hamiltonian for a semi-infinite chain reads

$$H_{XXZ} = - \sum_{l=0}^{\infty} \{ J (S_l^x S_{l+1}^x + S_l^y S_{l+1}^y) + J_z S_l^z S_{l+1}^z \}. \quad (1.1)$$

We focus on (normalized) spin-autocorrelation functions

$$C^{\mu\mu}(t) \equiv \frac{\langle S_l^\mu(t) S_l^\mu \rangle}{\langle S_l^\mu S_l^\mu \rangle}, \quad \mu = x, z \quad (1.2)$$

at $T = \infty$ and the associated spectral densities

$$\Phi_l^{\mu\mu}(\omega) \equiv \int_{-\infty}^{+\infty} dt e^{i\omega t} C_l^{\mu\mu}(t), \quad \mu = x, z. \quad (1.3)$$

Results will be presented for $l = \infty$ (bulk spin) and $l = 0$ (boundary spin). For two special cases, the dynamics can be analyzed exactly: the XX model ($J_z = 0$) is equivalent to a system of noninteracting lattice fermions, and the X model ($J = 0$) is as trivial as the quantum harmonic oscillator. For other parameter values, however, the $T = \infty$ dynamics of the XXZ model is quite complicated, and transitions between different types of dynamical behavior can be studied. For that purpose, the two above-mentioned methods (i) and (ii) of analyzing frequency moments turn out to be invaluable instruments for analysis and interpretation. Our main point of emphasis is the identification of diffusive long-time tails in spin-autocorrelation functions under the right symmetry conditions or the corresponding infrared divergences in the associated spectral densities.

The phenomenon of spin diffusion is based on a thermalization process that is subject to a conservation law. The phenomenological theory in its simplest form states that the fluctuations $S^\mu(q, t)$ of any conserved spin component satisfy the diffusion equation for sufficiently long times and wavelengths. It predicts exponential decay for correlation functions that are not constrained by that conservation law and diffusive long-time tails for those that are. The fact is that exponential decay in time or diffusive long-time tails do not occur in any of the

known exact results for interacting quantum spin systems. The decay in those systems turns out to be either Gaussian or nondiffusive power law. In this study we provide evidence in support of spin diffusion in the 1D $s = \frac{1}{2}$ XXZ model in the form of a crossover from Gaussian to exponential decay (Sec. III) and in the form of long-time tails that come and go with the conservation law required for diffusive behavior (Secs. IV–VI). The presentation of the results is preceded (Sec. II) by a brief description of the two main methods of analysis employed here.

II. CALCULATIONAL TECHNIQUES

At $T = \infty$, the spin-autocorrelation function (1.2) is real and symmetric. It can be expanded into a power series of the form

$$C_l^{\mu\mu}(t) = \sum_{k=0}^{\infty} \frac{(-1)^k}{(2k)!} M_{2k}^{\mu\mu}(l) t^{2k}, \quad (2.1)$$

where the expansion coefficients are the frequency moments of the spectral density (1.3)

$$\begin{aligned} M_{2k}^{\mu\mu}(l) &= \int_{-\infty}^{+\infty} \frac{d\omega}{2\pi} \omega^{2k} \Phi_l^{\mu\mu}(\omega) \\ &= (-1)^k \left[\frac{d^{2k}}{dt^{2k}} C_l^{\mu\mu}(t) \right]_{t=0}, \quad k = 0, 1, 2, \dots, \end{aligned} \quad (2.2)$$

and can be expressed as expectation values

$$M_{2k}^{\mu\mu}(l) = -(-1)^k \langle [\dots [S_l^\mu, H], \dots, H] [\dots [S_l^\mu, H], \dots, H] \rangle / \langle S_l^\mu S_l^\mu \rangle \quad (2.3)$$

of operators produced by the product of two k -fold commutators.^{5,25} These expectation values can be evaluated exactly by readily programmable integer arithmetic as explained in Ref. 25. We have determined the $M_{2k}^{\mu\mu}(l)$ up to $k = 14$ for the bulk spin ($l = \infty$) of the XXZ model and up to $k = 17$ for the boundary spin ($l = 0$). This represents a significant advance from previously known moments for that model.^{5,24} The exact moments are listed in Appendix A.

In Sec. III we shall use these expansion coefficients to determine upper and lower bounds of the spin-autocorrelation function by methods that have been developed and described previously.^{5,24–27} In Secs. IV–VI the information contained in the frequency moments will be analyzed by quite different methods. We convert the $M_{2k}^{\mu\mu}(l)$ into the continued-fraction coefficients $\Delta_k^{\mu\mu}(l)$ of the relaxation function

$$c_l^{\mu\mu}(z) \equiv \int_0^\infty dt e^{-zt} C_l^{\mu\mu}(t) = \frac{1}{z + \frac{\Delta_1^{\mu\mu}(l)}{z + \frac{\Delta_2^{\mu\mu}(l)}{z + \dots}}}, \quad (2.4)$$

which is the Laplace transform of the spin-autocorrelation function (1.2), and proceed with the

analysis from there. A set of transformation formulas between the first K frequency moments $M_{2k}^{\mu\mu}(l)$ and the first K coefficients $\Delta_k^{\mu\mu}(l)$ is given in Appendix B.

It must be mentioned that the continued-fraction coefficients $\Delta_k^{\mu\mu}(l)$ can be determined more directly by means of the recursion method. The computational effort is almost identical to that required for the determination of an equal number of frequency moments $M_{2k}^{\mu\mu}(l)$. A brief account of Lee's²⁸ formulation of the recursion method as applied to quantum spin dynamics at high temperature was given in Refs. 15, 21, and 23 for several applications.

In this paper, the known continued-fraction coefficients $\Delta_k^{\mu\mu}(l)$ will be analyzed along two different lines: (a) We shall reconstruct the spectral density (1.3) from the relaxation function (2.4) via the relation

$$\Phi_l^{\mu\mu}(\omega) = 2 \lim_{\epsilon \rightarrow 0} \mathcal{R}[c_l^{\mu\mu}(\epsilon - i\omega)] \quad (2.5)$$

by methods involving the use of matching termination functions that have previously been tested and applied in quantum spin dynamics.^{23,29,30} (b) We shall employ the method developed in Ref. 30 for the identification of infrared singularities in spectral densities by direct analysis of the known sequence of $\Delta_k^{\mu\mu}(l)$.

III. FROM GAUSSIAN DECAY TO EXPONENTIAL RELAXATION

Consider first the bulk-spin autocorrelation function $\langle S_\infty^x(t)S_\infty^x \rangle$ of the XXZ model (1.1). The nontrivial but exactly solvable case $J_z = 0$ (XX model) is an ideal starting point for the analysis of the XXZ cases by both calculational techniques we intend to employ. The well-known exact expressions for that autocorrelation function and its spectral density in the XX limit read:¹⁸⁻²¹

$$\langle S_\infty^x(t)S_\infty^x \rangle = \langle S_\infty^y(t)S_\infty^y \rangle = \frac{1}{4}e^{-J^2 t^2/4}, \quad (3.1)$$

$$\Phi_\infty^{xx}(\omega) = \frac{2\sqrt{\pi}}{J} e^{-\omega^2/J^2}. \quad (3.2)$$

The Gaussian decay of (3.1) is clearly anomalous, attributable to the free-fermion nature of the XX model. The default expectation within the spin-diffusion scenario would be exponential decay at long times instead. The nongeneric processes that govern the transport of spin fluctuations in the XX model are further indicated by the fact that all pair-correlation functions $\langle S_i^x(t)S_{i'}^x \rangle$, $i \neq i'$ are identically zero. In the XXZ model, the anomalous features are expected to disappear. A weak fermion interaction (with coupling constant J_z) impacts the long-time behavior more strongly than it affects the short-time behavior. In the function $\langle S_\infty^x(t)S_\infty^x \rangle$ we thus expect to see a crossover from a Gaussian behavior at short times to exponential decay at longer times. The very simple structure of the exact result (3.1) makes it possible to observe clear indicators for such a crossover in a short-time expansion at $J_z \ll J$.

In Fig. 1 we have plotted the function $\ln(\langle S_\infty^x(t)S_\infty^x \rangle) / (Jt \langle S_\infty^x S_\infty^x \rangle)$ versus Jt for four

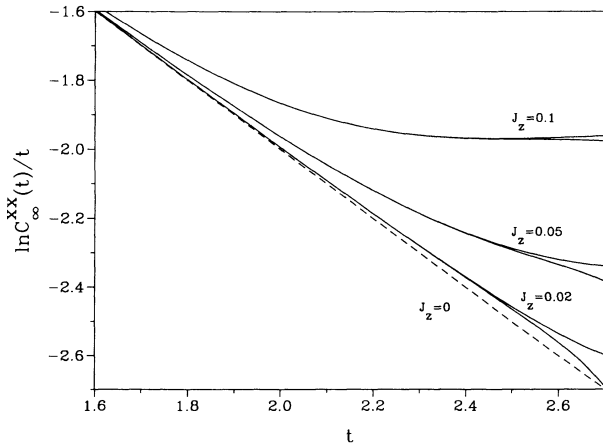


FIG. 1. Short-time expansion of the spin-autocorrelation function $C_\infty^{xx}(t) = \langle S_\infty^x(t)S_\infty^x \rangle / \langle S_\infty^x S_\infty^x \rangle$ at $T = \infty$ of the 1D $s = \frac{1}{2}$ XXZ model for $J = 1$ and $J_z = 0.02, 0.05, 0.1$ (solid lines) near the exactly solvable case $J_z = 0$ (dashed line). The data are plotted in a way suitable for visualizing the crossover from Gaussian decay (negative unit slope) to exponential decay (zero slope). Each result of the short-time expansion is represented by two curves corresponding to an upper and a lower bound of the function. The bounds have been determined from 14 exact frequency moments $M_{2k}^{xx}(\infty)$.

different parameter values of the XXZ model near the XX limit. The straight dashed line with negative slope represents the pure Gaussian (3.1). The results for $J_z \neq 0$ show strong indications that the decay is slower than Gaussian, consistent with exponential decay (convergence toward a negative constant in the plot of Fig. 1). Power-law decay would imply convergence toward zero. Whether or not the observed exponential decay represents the true asymptotic behavior is, of course, beyond the reach of this type of analysis.

IV. FROM EXPONENTIAL RELAXATION TO DIFFUSIVE LONG-TIME TAILS

Unlike in classical spin dynamics, where diffusive long-time tails are readily detectable in simulation data and directly amenable to a quantitative analysis, the most direct indicators of their presence in quantum spin dynamics (at least in 1D and 2D systems) are infrared divergences in spectral densities. The continued-fraction analysis is an ideal instrument for the quantitative study of such singularities.

A. Δ_k sequences and model spectral densities

The exact result (3.2) for the spectral density $\Phi_\infty^{xx}(\omega)$ of the XX model can be reproduced by means of the recursion method with relative ease. It is determined by the linear sequence

$$\Delta_k^{xx}(\infty) = \frac{1}{2}J^2 k \quad (J_z = 0) \quad (4.1)$$

via (2.4) and (2.5).²¹ The strength of the continued-fraction analysis of this function derives from the fact that gradual deviations from the exactly solvable limit $J_z = 0$ produce only gradual deviations from (4.1). The resulting nearly linear Δ_k sequences, in turn, produce gradual changes in the spectral density $\Phi_\infty^{xx}(\omega)$.

As J_z increases from zero, we can identify two types of systematic deviations of the Δ_k 's from the linear sequence (4.1): (i) A gradual increase in growth rate λ implies a gradual change in the decay law at large ω of the spectral density according to the following relation:^{31,32}

$$\Delta_k^{\mu\mu}(l) \sim k^\lambda \iff \Phi_l^{\mu\mu}(\omega) \sim \exp(-|\omega|^{2/\lambda}). \quad (4.2)$$

(ii) Gradually increasing alternating deviations of the Δ_k 's from the line k^λ signal the emergence of a power-law singularity at $\omega = 0$ in the spectral density and allow for an estimate of the singularity exponent.^{23,30} Both effects are illustrated in Fig. 2. The main plot shows $\ln \Delta_k$ versus $\ln k$ for two cases of the XXZ model. The open circles represent the linear sequence (4.1) for $J_z = 0$, which has slope $\lambda = 1$. The regression line for $J_z = J$ has slope $\lambda \approx 1.22$. The predominantly alternating deviations of the full circles from that line are clearly visible. The inset shows the variation of the growth rate λ with J_z between the XX and XXX models.³³ Changes in growth rate over that range have only negligible impact on the physically interesting structures in the spectral densities investigated here. The growing alternating deviations in the Δ_k sequence are the signature of an emerging infrared divergence implied by the spin-diffusive long-time tail that is

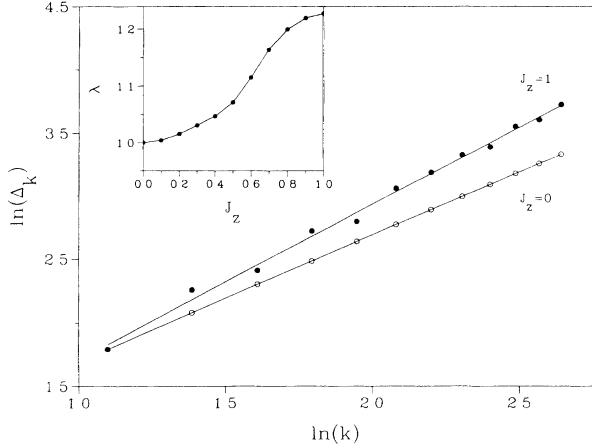


FIG. 2. Log-log plot of the sequences $\Delta_k^{xx}(\infty)$ for the bulk-spin-autocorrelation function $\langle S_\infty^x(t)S_\infty^x \rangle$ at $T = \infty$ of the 1D $s = \frac{1}{2}$ XX model ($J = 1, J_z = 0$) and XXX model ($J = J_z = 1$). The slope of the linear regression lines determines the growth rate λ of each Δ_k sequence. The inset shows λ as a function of J_z (for $J = 1$).

expected to dominate the function $\langle S_\infty^x(t)S_\infty^x \rangle$ for $J_z = J$. A quantitative analysis of that singularity will be presented in Sec. IV C. It yields strong evidence for a transition from an unconstrained relaxation process at $J_z < J$ to a diffusion process at $J_z = J$ in the fluctuations of $S_\infty^x(t)$.

For the reconstruction of spectral densities from Δ_k sequences with growth rates $\lambda \simeq 1$, we have proposed and successfully employed the following procedure:^{29,30} (i) Pick a Gaussian model spectral density, $\bar{\Phi}(\omega) = (2\sqrt{\pi}/\omega_0)\exp(-\omega^2/\omega_0^2)$. (ii) Expand the associated model relaxation function (2.4) into a continued fraction down to level n ; this generates the model coefficients $\bar{\Delta}_k = \omega_0^2 k/2$ and defines the n th-level termination function $\Gamma_n(z)$. (iii) Determine the parameter ω_0 by matching the slope of $\bar{\Delta}_k$ versus k with the average slope of $\Delta_k^{xx}(\infty)$ vs k for the finite sequence of coefficients $\Delta_1^{xx}(\infty), \dots, \Delta_n^{xx}(\infty)$ pertaining to the dynamical quantity of interest and inferred from exact moments or produced by the recursion method. (iv) Replace the model coefficients $\bar{\Delta}_1, \dots, \bar{\Delta}_n$ by the known system coefficients $\Delta_1^{xx}(\infty), \dots, \Delta_n^{xx}(\infty)$ in the relaxation function and evaluate the spectral density via (2.5). That is the recipe for reconstructing spectral densities by means of a *Gaussian terminator*.

For Δ_k sequences whose growth rates deviate significantly from $\lambda = 1$ and whose spectral densities are likely to have infrared divergences as their dominant structure we should carry out such an analysis on the basis of the more general model spectral density

$$\bar{\Phi}(\omega) = \frac{2\pi/\lambda\omega_0}{\Gamma\left[\frac{\lambda}{2}(1+\alpha)\right]} \left| \frac{\omega}{\omega_0} \right|^\alpha \exp(-|\omega/\omega_0|^{2/\lambda}). \quad (4.3)$$

This remains impractical as long as we lack closed-form expressions for the model continued-fraction coefficients Δ_k pertaining to (4.3) as functions of the three param-

eters $\omega_0, \alpha, \lambda$. However, for growth rates sufficiently close to $\lambda = 1$, we can approximate the ($\lambda \neq 1$) problem with a ($\lambda = 1$) problem if we replace the Δ_k sequence by the rescaled sequence

$$\Delta_k^* = \Delta_k^{1/\lambda} \quad (4.4)$$

and then proceed as outlined previously. The main distortions in the reconstructed spectral density caused by this approximation are of two kinds: (i) a change in the large- ω decay law and (ii) a change in the frequency scale. Whereas the former effect has only a negligible impact on the shape of the spectral-weight distribution, the latter may warrant attention and lead to significant improvement upon proper adjustment.³⁴

B. Reconstruction of spectral densities

We have reconstructed the bulk-spin spectral density $\Phi_\infty^{xx}(\omega)$ of the XXZ model for $0 \leq J_z/J \leq 1$ by using the continued-fraction coefficients $\Delta_1^{xx}(\infty), \dots, \Delta_{14}^{xx}(\infty)$ inferred from the moments tabulated in Appendix A and a Gaussian terminator with its parameter determined from the slope of the Δ_k^* sequence.

Figure 3 shows the reconstructed function $\Phi_\infty^{xx}(\omega)$, at $\omega < 0$ for values of the anisotropy parameter between $J_z/J = 0$ and $J_z/J = 0.5$, and at $\omega > 0$ for parameter values between $J_z/J = 0.6$ and $J_z/J = 1.0$. The five curves on the left illustrate how the pure Gaussian (3.2) (dashed line) evolves into a curve with some structure as J_z/J increases from zero. The additional structure consists of (i) a central peak of increasing height and decreasing width and (ii) a shoulder of enhanced spectral weight

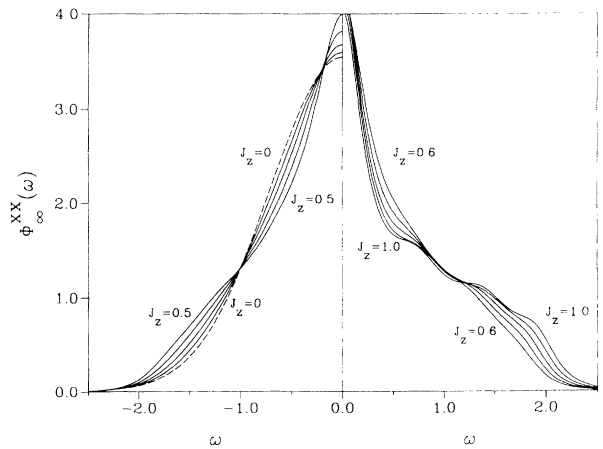


FIG. 3. Spectral density $\Phi_\infty^{xx}(\omega)$ at $T = \infty$ of the 1D $s = \frac{1}{2}$ XXZ model with $J = 1$ as reconstructed from the continued-fraction coefficients $\Delta_1^{xx}(\infty), \dots, \Delta_{14}^{xx}(\infty)$ and a Gaussian terminator. The calculation was carried out by the use of the Δ_k^* sequence in the role of the original Δ_k sequence. The four solid curves for $\omega < 0$ pertain to the values $J_z = 0.2, \dots, 0.5$ of the anisotropy parameter and the five curves plotted for $\omega > 0$ to values $0.6, \dots, 1.0$. The dashed curve represents the exact result (3.2) for the case $J_z = 0$. The result for $J_z = 0.1$ (not shown) deviates from that for $J_z = 0$ by amounts comparable to the thickness of the dashed line.

at $\omega \simeq 1.5J$. The further development of the spectral density as J_z/J approaches the XXX case is shown by the curves on the right. The shoulder becomes more pronounced, and the strong peak at $\omega=0$, signals the presence of an infrared divergence for $J_z=J$ in accordance with spin-diffusion phenomenology.

The curve for the XXX case is in qualitative agreement with previous results obtained from finite-chain calculations,^{3,4} and by a calculation which uses the first two frequency moments of the dynamic structure factor in conjunction with a two-parameter diffusivity.⁶ We should like to emphasize that the infrared singularity in $\Phi_\infty^{xx}(\omega)$, which is strongly suggested by the curves for $J_z/J \simeq 1$ in Fig. 3, is in no way artificially built into our approach. It is a structure resulting solely from the 14 known continued-fraction coefficients.

The reconstructed spectral density $\Phi_\infty^{xx}(\omega)$ shown in Fig. 3 is expected to be most accurate for small values of J_z/J , where the growth rate is closest to $\lambda=1$ (see Fig. 2, inset). As the growth rate increases toward $\lambda \simeq 1.22$, the curves are likely to become subject to the above-mentioned systematic errors. We have estimated the systematic error in frequency scale not to exceed 2% for the curves at $0 < J_z/J \leq 0.5$ and 12% for those at $0.5 < J_z/J \leq 1$.

C. Analysis of infrared singularities

For a quantitative analysis of the infrared singularity in the spectral density $\Phi_\infty^{xx}(\omega)$, we focus on the alternating deviations about the average (nearly linear) growth of the Δ_k sequences. Consider the special case $\lambda=1$ of the model spectral density (4.3). The associated Δ_k sequence is known in closed form:²⁹

$$\bar{\Delta}_{2k-1} = \frac{1}{2}\omega_0^2(2k-1+\alpha), \quad \bar{\Delta}_{2k} = \frac{1}{2}\omega_0^2(2k). \quad (4.5)$$

For this model spectral density, the singularity exponent α is determined by the displacement of the $\bar{\Delta}_{2k-1}$ from the line $\bar{\Delta}_{2k} = \omega_0^2 k$. In real situations, that displacement is subject to "fluctuations" caused by other structures in the spectral density. The exponent α of the infrared singularity can nevertheless be estimated from the average distance in vertical displacement of the Δ_{2k} and the Δ_{2k-1} from the linear regression line for the entire sequence. Two previous applications of that procedure yielded reasonable results.^{23,30}

The results of such an analysis applied to the Δ_k^* sequences inferred from 14 exact moments are compiled in Fig. 4. The full circles joined by solid lines represent the mean exponent values α as a function of J_z/J ranging from the XX model ($J_z=0$) to the XXX model ($J_z=J$) and somewhat beyond. The error bars indicate the statistical uncertainty for each data point, which is due to the fact that the analysis is based on a finite number of known continued-fraction coefficients. On top of the statistical error, the data are likely to be subject to a systematic error whose potential impact increases with the deviation of the growth rate from $\lambda=1$. We have yet to design a simple and satisfactory way to correct for systematic errors in the exponent analysis. As J_z ap-

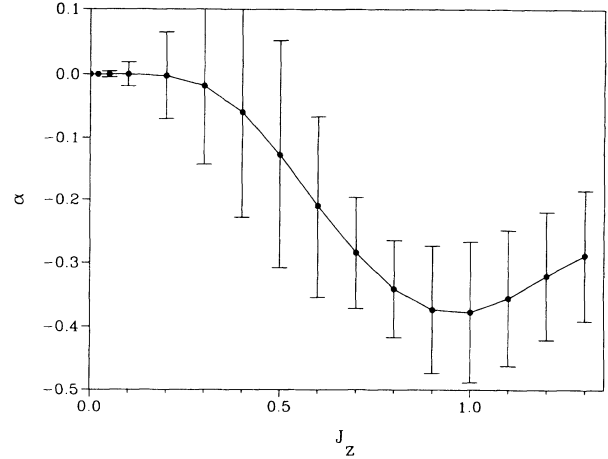


FIG. 4. Infrared-singularity exponent α versus anisotropy parameter J_z of the spectral density $\Phi_\infty^{xx}(\omega)$ at $T = \infty$ of the 1D $s = \frac{1}{2} XXZ$ model with $J=1$. The data points were obtained from the continued-fraction coefficients $\Delta_3^{xx}(\infty), \dots, \Delta_{14}^{xx}(\infty)$ by analyzing the associated Δ_k^* sequence.

proaches zero, both types of uncertainties (statistical and systematic) become smaller and disappear. The data point $\alpha(0)=0$ is exact and describes the spectral density (3.2), which has no infrared singularity.

In spite of the limited overall accuracy of these results, the dependence on J_z/J of the mean exponent values displayed in Fig. 4 is quite remarkable. The data strongly indicate that the function $\alpha(J_z/J)$ stays zero over some range of the anisotropy parameter. A vanishing exponent at small but nonzero J_z/J is consistent with and thus reinforces the conclusion reached from the short-time analysis that the function $\langle S_\infty^x(t)S_\infty^x \rangle$ decays faster than a power law.

While the data point at $J_z/J=0.5$ is still consistent with $\alpha=0$, the mean α values have already a strongly decreasing trend at this point. A minimum value is reached exactly at the symmetry point ($J_z=J$) of the XXX model—the only point for which the conservation law $S_T^x = \sum_i S_i^x = \text{const}$ holds, and therefore the only point for which one expects a diffusive long-time tail in $\langle S_\infty^x(t)S_\infty^x \rangle$. Upon further increase of J_z/J , the data points rise again toward $\alpha=0$ as expected.

The minimum exponent value, $\alpha = -0.37 \pm 0.12$, obtained for the XXX case is only marginally consistent with the standard value, $\alpha = -\frac{1}{2}$, predicted by spin-diffusion phenomenology. That discrepancy is more likely attributable to the systematic error in our data than it is evidence for anomalous spin diffusion such as was discovered in the classical 1D XXX model.⁷⁻¹³

V. SUSTAINED POWER-LAW DECAY

The conservation law $S_T^z = \sum_i S_i^z = \text{const}$ for the spin fluctuations in the z direction holds over the entire parameter range of the XXZ model. Consequently, the long-time behavior of the correlation function $\langle S_\infty^z(t)S_\infty^z \rangle$ or the low-frequency behavior of the spectral density $\Phi_\infty^{zz}(\omega)$ is expected to be much less affected by

the symmetry change of H_{XXZ} at $J_z=J$ than the functions $\langle S_\infty^x(t)S_\infty^x \rangle$ and $\Phi_\infty^{XX}(\omega)$ were. The verification of sustained power-law decay at $J_z \neq J$ as a contrast to the results presented in Sec. IV will further support the case for quantum spin diffusion.

Here the kind of analysis carried out previously for the reconstruction of spectral densities (Sec. IV B) and for the estimation of singularity exponents (Sec. IV C) becomes inapplicable for $0 \leq J_z/J \leq 0.6$. The breakdown is caused by a crossover in the growth rates of the relevant sequences of continued-fraction coefficients. Figure 5 shows the Δ_k sequences plotted versus k of $\Phi_\infty^{zz}(\omega)$ for four different parameter values. Between $J_z/J=0.6$ and $J_z/J=1.0$, the sequence of known coefficients has a well defined growth rate somewhat in excess of $\lambda=1$. For the XX model ($J_z=0$), on the other hand, growth rate $\lambda=0$ is well known to be realized.^{5,23} The sequence for $J_z/J=0.1$ has attributes of both regimes. It starts out with $\lambda=0$ up to $k \simeq 7$ and then begins to grow with $\lambda \gtrsim 1$, thus causing a kink in Δ_k versus k . That is so throughout the range $0 < J_z/J < 0.6$. It is impossible to analyze such sequences on the basis of a unique value of λ , and, therefore, impossible to carry out the analysis described before without major modifications.³⁵

The bulk-spin spectral density $\Phi_\infty^{zz}(\omega)$ for four parameter values over the range $0.7 \leq J_z/J \leq 1.0$ as reconstructed from the 14 known Δ_k 's and a Gaussian terminator with its parameter from the Δ_k^* sequence is displayed in Fig. 6 (solid curves). Notice how the shape of the functions $\Phi_\infty^{zz}(\omega)$ (Fig. 6) and $\Phi_\infty^{xx}(\omega)$ (Fig. 3), which start out identically, undergo different changes as the anisotropy parameter decreases from $J_z/J=1$. While the function $\Phi_\infty^{xx}(\omega)$ gradually transforms into a pure Gaussian (dashed line in Fig. 3), the function $\Phi_\infty^{zz}(\omega)$ is supposed to approach the exact result¹⁷

$$\Phi_\infty^{zz}(\omega) = \frac{2}{\pi J} K(\sqrt{1-\omega^2/4J^2}) \Theta(1-\omega^2/4J^2) \quad (J_z=0). \quad (5.1)$$

The graph of that complete elliptic integral has been added as dashed line to Fig. 6. The diminishing height of the central peak with decreasing J_z/J marks the weakening of the divergence from $\sim \omega^{-1/2}$ (diffusive) to $\sim \ln(1/\omega)$ (free fermions). Spectral weight removed from the central peak and from the high-frequency tail is transferred to the shoulder, which gradually transforms into a discontinuity at $\omega/J=2$.

The inset to Fig. 6 shows our results for the infrared singularity exponent α over the parameter range $0.6 \leq J_z/J \leq 1.5$. Within the statistical uncertainties indicated by error bars, the data points are consistent with a J_z -independent exponent. This confirms that the fluctuations of S_i^z are largely unaffected by the change in the symmetry at $J_z/J=1$ in strong contrast to our observations made in Fig. 4 for the fluctuations of S_i^x . The weak monotonic J_z dependence of the mean exponent values at $J_z/J \geq 0.8$ and their deviation from the standard value $\alpha=-0.5$ are probably attributable to the previously mentioned systematic errors, which we have not fully under control. However the sloping tendency of the mean values toward the lowest values of J_z , and the extra large error bars on those data points are an artifact caused by the crossover between growth rates as discussed in the context of Fig. 5.

VI. BOUNDARY-SPIN SPECTRAL DENSITIES

The conclusions drawn in Secs. IV and V for the bulk-spin spectral densities $\Phi_\infty^{xx}(\omega)$ and $\Phi_\infty^{zz}(\omega)$ are further sub-

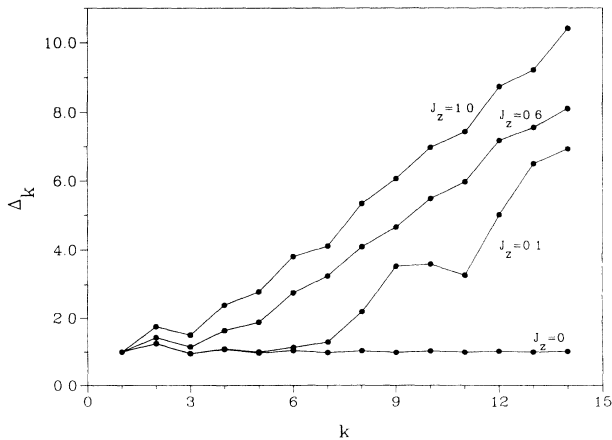


FIG. 5. Continued-fraction coefficients $\Delta_k^z(\infty)$ vs k for the bulk-spin-autocorrelation function $\langle S_\infty^z(t)S_\infty^z \rangle$ at $T=\infty$ of the 1D $s=\frac{1}{2}$ XXZ model with $J=1$ and $J_z=0$ (XX case), $J_z=0.1$, 0.6 , and $J_z=1.0$ (XXX case). The kink of the sequence for $J_z=0.1$ illustrates the crossover between growth rates $\lambda=0$ and $\lambda \gtrsim 1$.

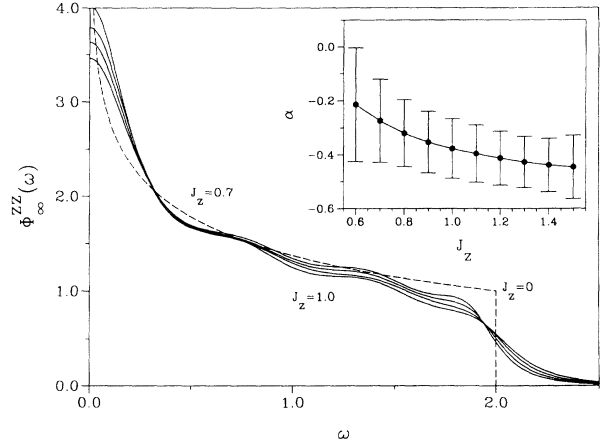


FIG. 6. Spectral density $\Phi_\infty^{zz}(\omega)$ at $T=\infty$ for the bulk-spin of the 1D $s=\frac{1}{2}$ XXZ model with $J=1$ as reconstructed from the continued-fraction coefficients $\Delta_1^z(\infty), \dots, \Delta_{14}^z(\infty)$ and a Gaussian terminator. The calculation was carried out by the use of the associated Δ_k^* sequence. The four solid curves represent the cases $J_z=0.7, 0.8, 0.9$, and 1.0 (XXX model). The dashed curve is the exact result (5.1) for $J_z=0$ (XX model). In the inset we have plotted the infrared-singularity exponent α vs J_z . The data points were obtained from $\Delta_3^z(\infty), \dots, \Delta_{14}^z(\infty)$ by analyzing the Δ_k^* sequence.

stantiated when we look at the results of the same analysis carried out for the boundary-spin spectral densities $\Phi_0^{\mu\mu}(\omega)$, $\mu=x,z$. For that calculation we have 17 Δ_k 's at our disposal (compared to 14 in the bulk case), but the problem with the λ crossover now plagues both x and z fluctuations for parameters $0 \leq J_z/J \leq 0.6$.

The spectral densities $\Phi_0^{xx}(\omega)$ for the cases $J_z/J=1.0, 0.6$ as reconstructed from the Δ_k^* sequence and a Gaussian terminator are shown in Fig. 7 (solid lines). The curve for the XXX case ($J_z=J$) shows a pronounced peak at $\omega=0$. That conspicuous enhancement of spectral weight has all but disappeared for $J_z/J=0.6$, i.e., in the presence of anisotropy, where S_T^z is not conserved. Hence the central peak in the XXX result can again be interpreted as a spin-diffusive divergence.

As the anisotropy parameter is decreased below the value $J_z/J=0.6$, the shape of the function $\Phi_0^{xx}(\omega)$ must approach that of the dashed line, which represents the exact result for $J_z/J=0$,^{22,23}

$$\Phi_0^{xx}(\omega) = (4/J) \sqrt{1 - \omega^2/J^2} \quad (J_z=0), \quad (6.1)$$

which is the Fourier transform of $\langle S_0^x(t) S_0^x \rangle = [J_0(Jt) + J_z(Jt)]/4$. While the Δ_k^* analysis breaks down for small values of J_z/J , the way the function $\Phi_0^{xx}(\omega)$ develops between $J_z/J=1.0$ and 0.6 can be extrapolated fairly smoothly toward the dashed line.

We have calculated the infrared-singularity exponent α of the boundary-spin spectral density $\Phi_0^{xx}(\omega)$ over the extended parameter range $0.6 \leq J_z/J \leq 1.2$ by means of the analysis explained previously. The inset to Fig. 7 shows seven equally spaced data points on that interval. The α values at the endpoints of the interval are very close to

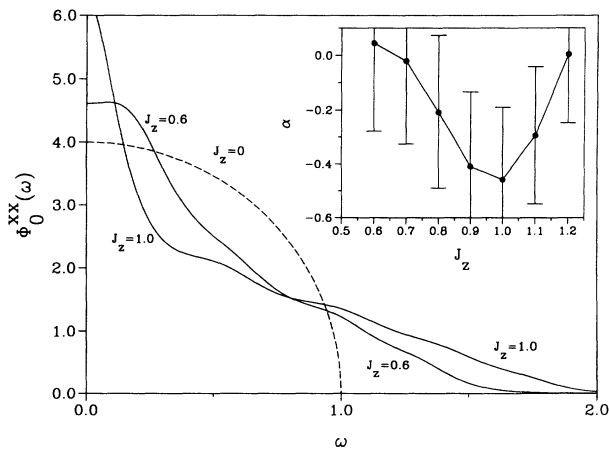


FIG. 7. Spectral density $\Phi_0^{xx}(\omega)$ at $T = \infty$ for the boundary spin of the semi-infinite 1D $s = \frac{1}{2}$ XXZ model with $J=1$ as reconstructed from the continued-fraction coefficients $\Delta_1^{xx}(0), \dots, \Delta_{17}^{xx}(0)$ and a Gaussian terminator. The calculation was carried out with the associated Δ_k^* sequence. The two solid curves represent the cases $J_z=1.0$ (XXX model) and $J_z=0.6$. The dashed curve is the exact result (6.1) for $J_z=0$ (XX model). In the inset we have plotted the infrared-singularity exponent α vs J_z . The data points were obtained from $\Delta_5^{xx}(0), \dots, \Delta_{17}^{xx}(0)$ by analyzing the Δ_k^* sequence.

zero. In between, the data points drop toward a minimum, again located at the symmetry point $J_z=J$, where the conservation law $S_T^z = \text{const}$ holds. The exponent value at the minimum, $\alpha = -0.45 \pm 0.26$, is consistent with spin-diffusion phenomenology.

Note the strongly contrasting J_z dependence of the singularity exponent pertaining to the spectral density $\Phi_0^{zz}(\omega)$ as shown in the inset to Fig. 8. Here the data points indicate the presence of an infrared divergence over the entire parameter range shown. However, a much stronger J_z dependence of the mean values of α is indicated than was the case of the corresponding bulk-spin results (Fig. 6). Whether that J_z dependence is entirely attributable to the systematic errors in our analysis and to the λ crossover remains to be seen.

In view of the fact that infrared divergences are likely to be real in the function $\Phi_0^{zz}(\omega)$ for all values of $J_z > 0$, we have treated them as such for its reconstruction from the known Δ_k 's. Instead of using a Gaussian terminator (cf. Sec. IV A), which is completely unbiased with respect to the spectral-weight distribution at low frequencies, we have used a two-parameter terminator with built-in infrared divergence. Its model relaxation function has been determined numerically via

$$\bar{c}(z) = \frac{1}{2\pi i} \int_{-\infty}^{+\infty} d\omega \frac{\bar{\Phi}(\omega)}{\omega - iz} \quad (6.2)$$

from the model spectral density (4.3) with $\lambda=1$. The value of the parameter ω_0 is determined by the slope of Δ_k versus k as before and the parameter α by our estimate of the singularity exponent.

Two of the curves in the main plot of Fig. 8 represent

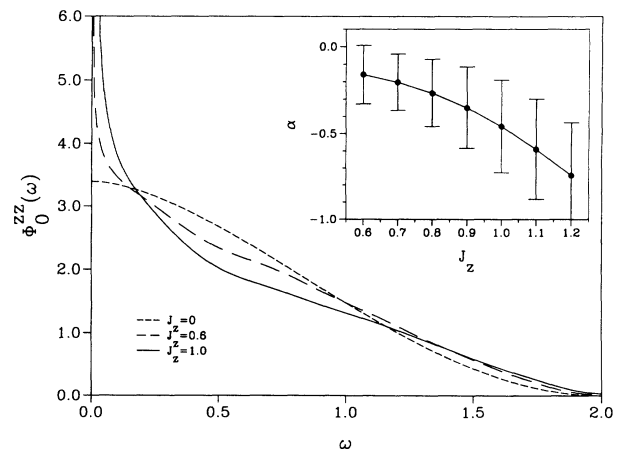


FIG. 8. Spectral density $\Phi_0^{zz}(\omega)$ at $T = \infty$ for the boundary spin of the semi-infinite 1D $s = \frac{1}{2}$ XXZ model with $J=1$ as reconstructed from the continued-fraction coefficients $\Delta_1^{zz}(0), \dots, \Delta_{17}^{zz}(0)$ and a special terminator with built-in infrared divergence. The calculation was carried out with the associated Δ_k^* sequence for the two cases $J_z=1.0$ (XXX model) and $J_z=0.6$. Also shown is the exact result (6.3) for $J_z=0$ (XX model). In the inset we have plotted the infrared-singularity exponent α vs J_z . The data points were obtained from $\Delta_5^{zz}(0), \dots, \Delta_{17}^{zz}(0)$ by analyzing the Δ_k^* sequence.

TABLE I. Coefficients $m_{2k}^{\infty, 2n}$ of the expansion (A1).

		(a)													
k	n	0	1	2	3	4	5	6	7	8	9	10			
	0	1	4	36	400	4900	63 504	853 776	11 778 624	165 636 900	2 363 904 400	34 134 779 536			
	1		8	8	220	4928	102 816	2 082 432	41 889 276	853 435 440	18 007 681 120	404 357 922 176			
	2				32	1680	65 040	2 202 552	69 951 024	2 185 202 448	70 013 058 128	2 392 462 416 032			
	3					128	10 944	690 624	36 246 496	1 698 825 024	75 435 121 632	3 333 426 429 472			
	4						512	64 768	6 755 840	549 482 752	37 407 224 320	2 310 521 698 496			
	5							2 048	359 424	68 143 104	8 681 526 272	845 021 416 448			
	6								8 192	1 904 640	773 124 096	149 994 047 488			
	7									32 768	9 748 480	10 104 356 864			
	8										131 072	48 562 176			
	9											524 288			
k	n												13	14	
	0												108 172 480 360 000	1 609 341 595 560 000	
	1												8 515 165 277 366 400	293 689 049 445 227 520	
	2												183 158 941 471 799 360	9 897 648 485 066 180 280	
	3												393 511 098 121 688 320	22 788 275 253 904 140 480	
	4												508 357 918 320 849 920	32 861 130 914 036 446 560	
	5												439 582 513 633 988 480	34 262 961 004 473 446 400	
	6												230 682 233 804 249 600	22 813 769 083 856 071 680	
	7												69 194 244 489 041 920	9 011 556 663 726 581 760	
	8												11 535 327 478 087 680	2 057 482 151 063 347 200	
	9												1 016 515 896 279 040	268 256 018 812 108 800	
	10												35 490 737 684 480	19 343 088 683 581 440	
	11												5 347 737 600	564 637 653 270 528	
	12												33 554 432	24 914 165 760	
	13													134 217 728	

TABLE II. Coefficients $m_{2k}^{2k}(\infty, 2n)$ of the expansion (A.1).

		(a)															
k	n	0	1	2	3	4	5	6	7	8	9	10					
	0	1	2	12	120	1680	30240	665280	17297280	518918400	17643225600	670442572800					
	1	2	24	24	260	3024	40320	680064	16024008	511299360	19380359856	790533972800					
	2	8	8	240	240	5012	96480	1863576	38116936	904349732	28564911232	1254507751744					
	3	32	32	32	32	1792	63744	1953776	56926012	1645089888	49127454896	1650071143616					
	4		128			128	11520	663872	31787392	1384501248	57265586368	2314444556752					
	5						512	67584	6456320	490989056	31918392704	1884787750016					
	6							2048	372736	65516544	8028291072	762099244032					
	7								8192	1966080	753139712	143168688128					
	8									32768	10027008	9966141440					
	9										131072	49807360					
	10											524288					
k	n													11	12	13	14
	0													28158588057600	1295295050649600	64764752532480000	3497296636753920000
	1													33192199504464	1410744469720768	60363991751481600	2604924609998538240
	2													67752201558496	3955582832037408	234928426159350720	13894163289895006800
	3													71440014187376	4224665438128064	306448398158942240	24028691547335252400
	4													94831675835968	4249623524974624	235784156426515200	17376963387911026200
	5													105259016639040	5715363282918656	310980152826272160	17917127977298169600
	6													62721972915712	4772749197832832	347319490135290880	24683103277934568960
	7													18825129374720	2069331679262720	207177188266183680	19623106832018688000
	8													2705189994496	465152129253376	65657336480194560	8385642509287802880
	9													145781686272	52188717776896	11232579986063360	1982528585053962240
	10													242221056	2247649132544	1005690153861120	262983884215418880
	11													2097152	1157627904	35458729902080	1918869792778304
	12														8388608	5452595200	564456232845312
	13															33554432	25367150592
	14																134217728

TABLE III. Coefficients $m_{2k}^z(0, 2n)$ of the expansion (A1).

k	(a)												(b)								
	n	0	1	2	3	4	5	6	7	8	9	10	11	12	n	13	14	15	16	17	
0	1	2	10	2	70	588	5544	56628	613470	6952660	81662152	987369656	12228193432	154532114800	0	1986841476000	25928281261800	342787130211150	4583937702039300	61923368957373000	
1	1	2	2	28	360	4752	4752	65494	940940	14014936	215358312	3404469096	55363106984	929065985440	1	16200874954800	296826867484110	5798385460938540	122683556698067640	2845789468891344360	
2	2	54	2	2	54	1166	1166	24310	515866	11203816	247345648	5523685016	124847197736	2872036690580	2	67890211103550	1669240405921410	1194139339025630880	35384641175890921200	106463055861804168000	
3	3	2	2	2	2	88	88	3172	107848	3651328	121432496	3906907224	121505574104	3685085980110	3	110439371747760	3319961677623180	3216997000723115040	171239371535145995280	172476952938667790880	
4	4	2	2	2	2	2	2	130	8422	476952	25617776	1263625096	56622505150	2337161324250	4	40826968637160	197777380312910	3968230388536813920	112937338652691902880	48167235794519032848	
5	5	2	2	2	2	2	2	2	180	24208	2201568	181559326	12792785196	769533217540	5	10024095487800	667749304798500	2166081794234685000	112937338652691902880	13216836286918095200	
6	6	2	2	2	2	2	2	2	2	238	78622	10508178	1301095050	127543927220	6	1267861285560	127114676648580	742482232802603520	48167235794519032848	2274442513310739376	
7	7	2	2	2	2	2	2	2	2	2	304	282764	50716840	9484170520	7	71037833760	12668494432980	156452354927034600	13216836286918095200	234196749152251744	
8	8	2	2	2	2	2	2	2	2	2	2	378	1079574	243836340	8	1160354160	551174008758	19392025540363632	13216836286918095200	2274442513310739376	
9	9	2	2	2	2	2	2	2	2	2	2	2	2	4239160	9	16840110	5457004878	1292809502109968	112937338652691902880	234196749152251744	
10	10	2	2	2	2	2	2	2	2	2	2	2	2	2	550	10	648	36982403631424	48167235794519032848	2274442513310739376	234196749152251744
11	11	2	2	2	2	2	2	2	2	2	2	2	2	2	2	11	754	116779829680	48167235794519032848	2274442513310739376	234196749152251744
12	12	2	2	2	2	2	2	2	2	2	2	2	2	2	2	12	2	116779829680	48167235794519032848	2274442513310739376	234196749152251744
13	13	2	2	2	2	2	2	2	2	2	2	2	2	2	2	13	2	116779829680	48167235794519032848	2274442513310739376	234196749152251744
14	14	2	2	2	2	2	2	2	2	2	2	2	2	2	2	14	2	116779829680	48167235794519032848	2274442513310739376	234196749152251744
15	15	2	2	2	2	2	2	2	2	2	2	2	2	2	2	15	2	116779829680	48167235794519032848	2274442513310739376	234196749152251744
16	16	2	2	2	2	2	2	2	2	2	2	2	2	2	2	16	2	116779829680	48167235794519032848	2274442513310739376	234196749152251744

the function $\Phi_0^{zz}(\omega)$ for $J_z/J=1.0$ and $J_z/J=0.6$ as reconstructed from the 17 known continued-fraction coefficients and this special terminator. As the parameter drops from the higher to the lower value, the central peak in the spectral density weakens considerably, and the weak shoulder at $\omega=J$ present for $J_z/J=1.0$ all but disappears. Upon further decrease of J_z/J to zero (XX model), the curve is supposed to approach the dashed line, which is the known exact result²³

$$\Phi_0^{zz}(\omega) = \frac{128}{3\pi J} (1 + \omega/2J) \left[\left(1 + \omega^2/4J^2 \right) E \left[\frac{2J - \omega}{2J + \omega} \right] - \frac{\omega}{J} K \left[\frac{2J - \omega}{2J + \omega} \right] \right]. \quad (6.3)$$

This limiting case is perfectly in line with how the reconstructed spectral density develops between $J_z/J=1.0$ and $J_z/J=0.6$.

ACKNOWLEDGMENTS

The work done at URI was supported by the U.S. National Science Foundation, Grants No. DMR-90-07540 and DMR-93-12252. Access to supercomputers at the National Center for Supercomputing Applications, University of Illinois Urbana-Champaign, is gratefully acknowledged. J.S. gratefully acknowledges support by the Max Kade Foundation. M.B. wishes to thank Hajo Leschke for helpful discussions and the Studienstiftung des deutschen Volkes for support.

APPENDIX A

The frequency moments (2.2) of the spectral density (1.3) as expressed in terms of the expectation values (2.3) yield upon evaluation, for the XXZ model (1.1), expressions of the form

$$M_{2k}^{\mu\mu}(l) = 2^{-2k} \sum_{n=0}^k m_{2k}^{\mu\mu}(l, 2n) J_z^{2n} J^{2(k-2n)} \quad (A1)$$

with integer coefficients $m_{2k}^{\mu\mu}(l, 2n)$. We have computed these coefficients up to $k=14$ for the bulk spin ($l=\infty$) and up to $k=17$ for the boundary spin ($l=0$). The former are listed in Table I for $\mu=z$ and Table II for $\mu=x$, the latter in Table III for $\mu=z$ and Table IV for $\mu=x$.

APPENDIX B

The first K expansion coefficients M_{2k} , $k=1, \dots, K$ of an autocorrelation function (1.2) (or frequency moments of its Fourier transform) determine the first K continued-fraction coefficients Δ_k , $k=1, \dots, K$ of its Laplace transform (2.4) and vice versa. The Δ_k , for example, are expressible in terms of Hankel determinants with elements consisting of moments M_{2k} .^{5,36,37} There exist several different algorithms for the numerical conversion of one set of numbers into the other. Some of them are more susceptible to numerical instabilities than others.³⁷ The following algorithm,³⁸ which is a product of the recursion method, has proven to be fairly robust against numerical instabilities in our applications:

Forward direction: For a given set of moments M_{2k} , $k=0, 1, \dots, K$ with $M_0=1$, the first K coefficients Δ_m , are determined by

$$M_{2k}^{(m)} = \frac{M_{2k}^{(m-1)}}{\Delta_{m-1}} - \frac{M_{2k-2}^{(m-1)}}{\Delta_{m-2}}, \quad \Delta_m = M_{2m}^{(m)} \quad (B1)$$

for $k=m, m+1, \dots, K$ and $m=1, 2, \dots, K$ and with set values $M_{2k}^{(0)} = M_{2k}$, $\Delta_{-1} = \Delta_0 = 1$, $M_{2k}^{(-1)} = 0$.

Reverse direction: For a given set of $\Delta_m = M_{2m}^{(m)}$, $m=1, \dots, K$, and $\Delta_{-1} = \Delta_0 = 1$, the moments $M_{2n}^{(0)} = M_{2n}$, result from the relations,

$$M_{2k}^{(m-1)} = \Delta_{m-1} M_{2k}^{(m)} + \frac{\Delta_{m-1}}{\Delta_{m-2}} M_{2k-2}^{(m-1)} \quad (B2)$$

for $m=k, k-1, \dots, 1$ and $k=1, 2, \dots, K$ and with set values $M_{2k}^{(-1)} = 0$.

*On leave from Institut für Physik, Universität Dortmund, D-44221 Dortmund, Germany. Present address: Lehrstuhl für Theoretische Physik I, Universität Bayreuth D-95440 Bayreuth, Germany.

¹D. Hone, C. Scherer, and F. Borsa, Phys. Rev. B **9**, 965 (1974); F. Borsa and M. Mali, *ibid.* **9**, 2215 (1974); J.-P. Boucher, M. Ahmed Bakheit, M. Nechtshein, M. Villa, G. Bonera, and F. Borsa, *ibid.* **13**, 4098 (1976).

²A. Lagendijk and E. Siegel, Solid State Commun. **20**, 709 (1976).

³F. Carboni and P. M. Richards, Phys. Rev. **177**, 889 (1969).

⁴J. P. Groen, T. O. Klaassen, N. J. Poulis, G. Müller, H. Thomas, and H. Beck, Phys. Rev. B **22**, 5369 (1980).

⁵J. M. R. Roldan, B. M. McCoy, and J. H. H. Perk, Physica A **136**, 255 (1986).

⁶R. A. Tahir-Kheli and D. G. McFadden, Phys. Rev. **178**, 800 (1969).

⁷G. Müller, Phys. Rev. Lett. **60**, 2785 (1988).

⁸R. W. Gerling and D. P. Landau, Phys. Rev. Lett. **63**, 812 (1989).

⁹G. Müller, Phys. Rev. Lett. **63**, 813 (1989).

¹⁰R. W. Gerling and D. P. Landau, Phys. Rev. B **42**, 8214 (1990).

¹¹J.-M. Liu, N. Srivastava, V. S. Viswanath, and G. Müller, J. Appl. Phys. **70**, 6181 (1991).

¹²O. F. De Alcantara Bonfim and G. Reiter, Phys. Rev. Lett. **69**, 367 (1992).

¹³M. Böhm, R. W. Gerling, and H. Leschke, Phys. Rev. Lett. **70**, 248 (1993).

¹⁴M. H. Lee, I. M. Kim, and R. Dekeyser, Phys. Rev. Lett. **52**, 1579 (1984); R. Dekeyser and M. H. Lee, Phys. Rev. B **43**, 8123, 8131 (1991).

¹⁵J.-M. Liu and G. Müller, Phys. Rev. A **42**, 5854 (1990).

¹⁶Th. Niemeijer, Physica **36**, 377 (1967).

- ¹⁷S. Katsura, T. Horiguchi, and M. Suzuki, *Physica* **46**, 67 (1970).
- ¹⁸A. Sur, D. Jasnow, and I. J. Lowe, *Phys. Rev. B* **12**, 3845 (1975).
- ¹⁹U. Brandt and K. Jacoby, *Z. Phys. B* **25**, 181 (1976).
- ²⁰H. W. Capel and J. H. H. Perk, *Physica* **87A**, 211 (1977); J. H. H. Perk and H. W. Capel, *ibid.* **89A**, 265 (1977).
- ²¹J. Florencio and M. H. Lee, *Phys. Rev. B* **35**, 1835 (1987).
- ²²S. Sen, *Phys. Rev. B* **44**, 7444 (1991).
- ²³J. Stolze, V. S. Viswanath, and G. Müller, *Z. Phys. B* **89**, 45 (1992).
- ²⁴U. Brandt and J. Stolze, *Z. Phys. B* **64**, 327 (1986).
- ²⁵M. Böhm and H. Leschke, *J. Phys. A* **25**, 1043 (1992).
- ²⁶M. Böhm and H. Leschke, *Physica A* **199**, 116 (1993); **203**, 328 (1994).
- ²⁷O. Platz and R. G. Gordon, *Phys. Rev. Lett.* **30**, 264 (1973); *Phys. Rev. B* **7**, 4764 (1973).
- ²⁸M. H. Lee, *Phys. Rev. Lett.* **49**, 1072 (1982); *Phys. Rev. B* **26**, 2547 (1982).
- ²⁹V. S. Viswanath and G. Müller, *J. Appl. Phys.* **67**, 5486 (1990).
- ³⁰V. S. Viswanath and G. Müller, *J. Appl. Phys.* **70**, 6178 (1991).
- ³¹A. Magnus, in *The Recursion Method and Its Applications*, edited by D. G. Pettifor and D. L. Weaire (Springer-Verlag, New York, 1985), p. 22.
- ³²D. S. Lubinsky, *Acta Appl. Math.* **10**, 237 (1987).
- ³³What looks like a gradual increase of λ may, in fact be a cross-over between two fixed values of growth rate, one for free fermions ($\lambda=0$) and another one for interacting fermions ($\lambda \simeq 1.2$). What counts for our analysis is the effective growth rate pertaining to the known finite Δ_k sequence.
- ³⁴It is no problem to design adjustments that remove some of the most obvious systematic errors in the results presented in Secs. IV–VI and to justify these corrections by very reasonable arguments. However, there is some ambiguity in how to implement these adjustments. This makes it hard to fully detach the choice of implementation from hindsight knowledge. We have decided, therefore, to present our results here without any such adjustments for systematic errors.
- ³⁵If the kink occurs at sufficiently large values of k , one might be tempted to analyze that Δ_k sequence on the basis of $\lambda=0$. The problem is that the interesting physics, caused by the effects of the fermion interaction for the case at hand, is contained in the Δ_k past the kink. Therefore, not much may be gained by such an exercise.
- ³⁶M. Dupuis, *Prog. Theor. Phys.* **37**, 502 (1967).
- ³⁷R. G. Gordon, *J. Math. Phys.* **9**, 655 (1968).
- ³⁸V. S. Viswanath and G. Müller, *Recursion Method—Applications to Many-Body Dynamics*, Lecture Notes in Physics, Vol. m23 [Springer-Verlag, New York, in press].